Electronic supplementary information for

In Situ Microbubbles Electroflotation Enhanced Emulsion Separation and Membrane Antifouling Ability for Durable Oil-in-Water Emulsion Separation

*Binyang Liu,[a] Peng Liu,[a] Jiahui Ye,[a] Yuqing Chen,[a] Xuesong Liu,[a] Wen Tian,[a] Junyi Ji,[a, b,] **

[a] School of Chemical Engineering, Sichuan University, Chengdu 610065, P. R. China

[b] State Key Laboratory of Polymer Materials Engineering, Sichuan University, Chengdu 610065, P. R. China

Corresponding author

Junyi Ji, E-mail: junyiji@scu.edu.cn

Supplementary Experimental Section

1. Materials

Titanium foam (pore size 5 μm) was purchased from Kunshan Guang Jiayuan Electronic Material Co., Ltd. Cobalt nitrate hexahydrate ($Co(NO_3)_2 \cdot 6H_2O$), ammonium fluoride (NH_4F), urea, anhydrous sodium sulfate (Na_2SO_4), isooctane, n-hexane, Petroleum ether, 1,2-dichloroethane, cetyltrimethylammonium bromide (CTAB), sodium dodecyl sulfonate (SDS), Tween 80, hydrochloric acid (HCl, 36%-38%), deionized (DI) water and ethanol were purchased from Chengdu Kelong Chemical Co. (Sichuan, China). Sudan IV and kerosene were purchased from Aladdin. Edible oil (cooking oil) was purchased from local supermarket. All the raw chemicals and materials were used without purification.

2. Characterizations

The surface morphology of as-prepared membranes was observed by scanning electron microscope (SEM, JEOL JSM-7610F). The elemental, phase structure and chemical composition information were determined by energy dispersive spectroscopy (EDS), X-ray diffraction (XRD, Rigaku), Raman spectroscopy (DXR, Thermo Fisher Scientific Co.) and X-ray photoelectron spectroscopy (XPS, PHI5000 Versa spectrometer), respectively. The contact angle measurement (DM-501) was used to measure the water contact angle (WCA) and underwater oil contact angle (UWOCA). The oil droplets in the filtrate were observed by optical microscope. The bubble-oil droplet interaction and the oil removal were observed by high-speed camera.

3. Electrochemical measurement.

The electrocatalytic performances of the OER were measured using an electrochemical station (CHI760E, Shanghai Chenhua Instrument Co., Ltd). The reactions were carried out in a standard three-electrode system with the electrodes as working electrode, graphite rods as counter electrode, and Ag/AgCl electrodes as reference electrode. Two different electrolytes, 1.0 M Na_2SO_4 and 0.2 M Na_2SO_4, were used, and the pH was about 7. All samples were scanned by cyclic voltammetry (CV) at 50 mV s^{-1} to obtain stable response current. All the measured potentials (vs. reference

electrode) were calculated with respect to reversible hydrogen electrode (RHE) by the Nernst equation ($E_{RHE} = E_M + 0.059 \times pH + E_R$), where E_M was the measured potentials, while E_R was 0.197 V for Ag/AgCl. The linear sweep voltammetry (LSV) curves were tested at 5 $mV \cdot s^{-1}$ with *iR* correction (The ohmic potential drop on the electrolyte resistance had been subtracted according to the equation: $E_{compensated} = E_M - i \times R_S$, R_S was determined by electrochemical impedance spectroscopy, EIS). Electrochemical impedance spectroscopy (EIS) spectra were recorded with frequency from 0.01 Hz to 100 kHz at an overpotential of 300 mV for OER. The electrochemical stability of the membrane was tested by chronopotentiometry at multi-current steps.

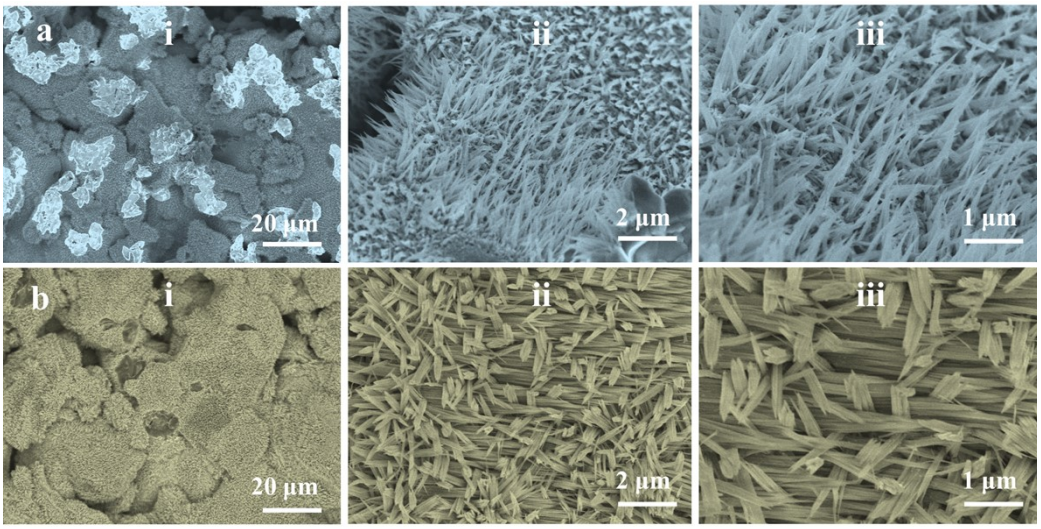

Fig. S1. Morphology of Co_3O_4 nanowires hydrothermal growth for (a) 4 h and (b) 8 h.

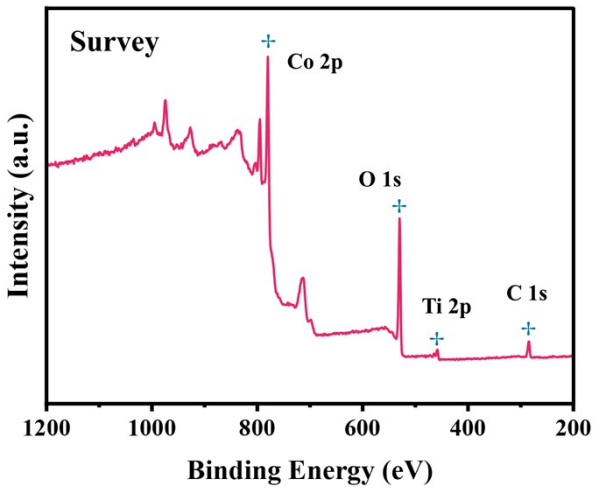

Fig. S2. XPS full survey spectra of CoTF.

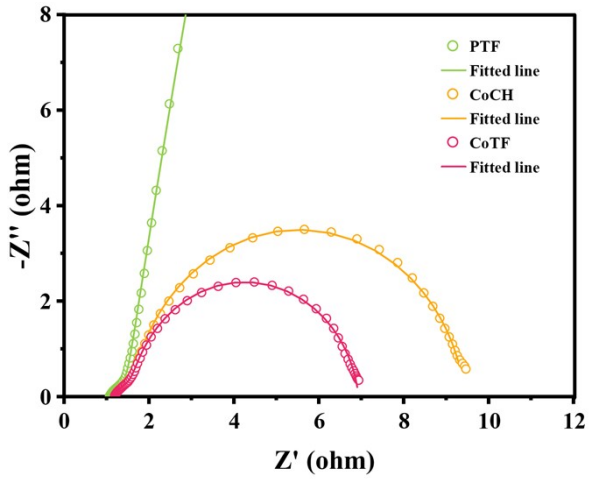

Fig. S3. Nyquist plots of PTF, CoCH and CoTF.

Fig. S4. Digital photographs of as-prepared SFE and SSE during a 6 day placement.

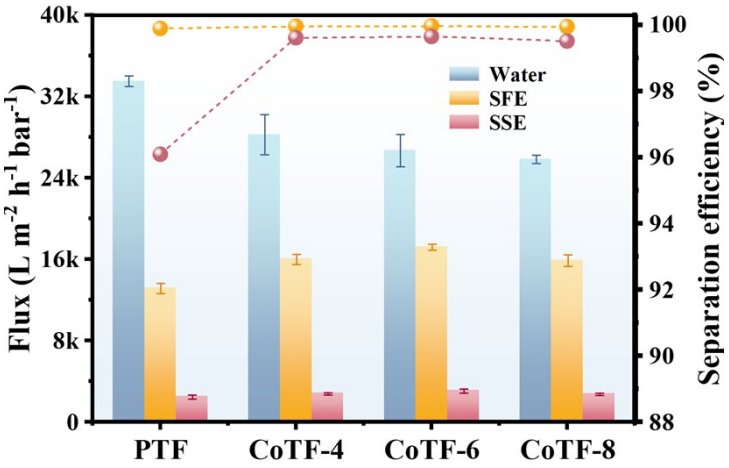

Fig. S5. Separation performance of PTF and CoTF-x grown under different hydrothermal times for pure water, SFE and SSE.

Without applied voltage, the emulsion separation performance of membranes with different hydrothermal time was investigated. As shown in **Fig. S5**, the pure water flux decreases with the increase of hydrothermal time, which can be due to the higher loading mass of Co_3O_4 nanowires resulting in the decrease of pore size. For the SFE separation, the separation efficiencies of the modified membranes are all above 99.9%, exhibiting excellent separation effect. With the increase of hydrothermal time, the flux of CoTF-6 increased from 16.05±0.50 kL m^{-2} h^{-1} bar^{-1} to 17.22±0.30 kL m^{-2} h^{-1} bar^{-1}, which is attributed to the antifouling capability of the closely shaped nanowire structure. However, the flux of CoTF-8 decreases to 15.92±0.56 kL m^{-2} h^{-1} bar^{-1}, which may be due to the overgrown nanowires blocking the pores. For the SSE separation, CoTF-6 also has the highest separation efficiency (99.6%) and flux (3.12±0.20 kL m^{-2} h^{-1} bar^{-1}). Therefore, CoTF-6 with well-grown nanostructure and optimal separation performance is selected for further study.

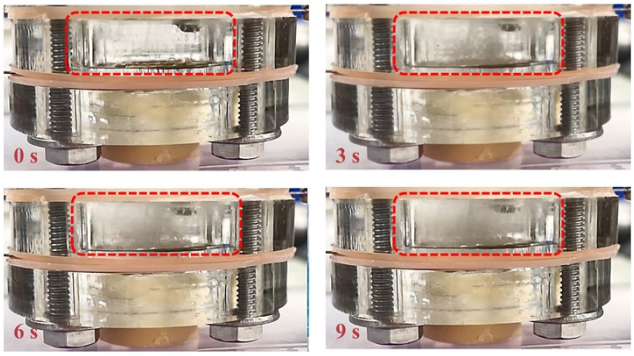

Fig. S6. Photos of bubble-generated on the membrane surface after applying 10 V voltage.

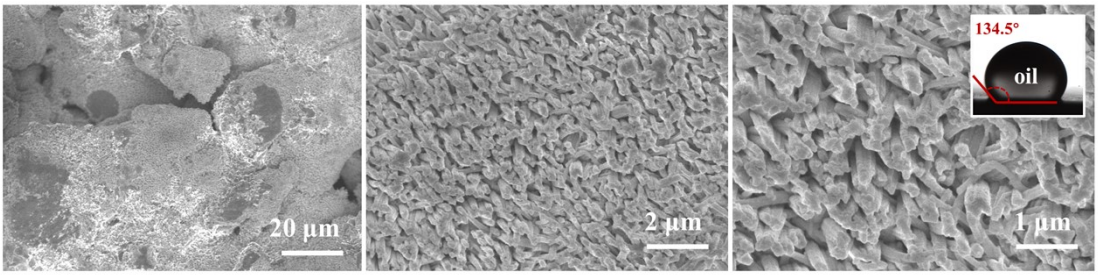

Fig. S7. SEM images of the surface morphology of CoTF membrane after long-term operation (inset shows the UWOCA of CoTF for 1,2-dichloromethane).

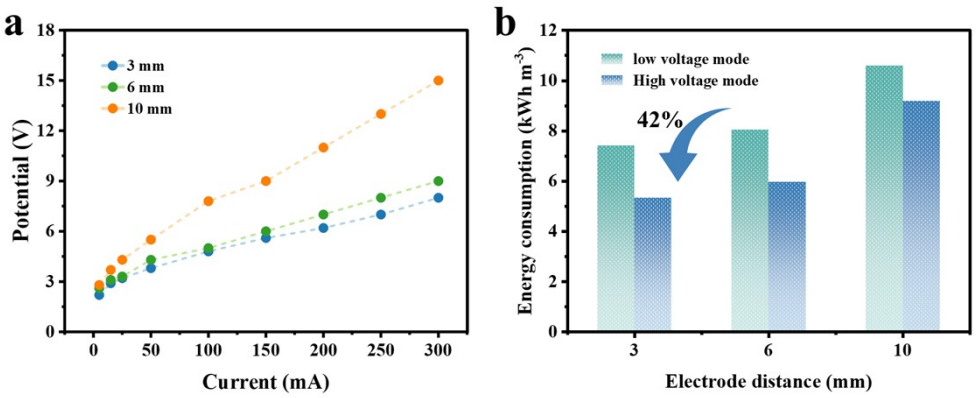

Fig. S8. (a) The trends of current variation with voltage at different electrode distances. (b) Energy consumption of oil-water emulsion separation in different voltage modes at different electrode distances.

The energy consumption of the device is further optimized via adjusting the electrode distance. As shown in **Fig. S8**, when the electrode distance is reduced from 10 mm to 3 mm, the current response of the system is substantially improved and the energy consumption is significantly reduced, achieving an energy reduction value of 42%. Meanwhile, compared with the 5 V continuous operation mode, the 10 V intermittent pulse operation exhibits a marked advantage in energy efficiency, with about 28.5% energy saving (different O/W emulsion treating volume under 5 or 10 V). This result reveals the potential of intermittent pulse operation in improving energy utilization efficiency for oil-water separation, which may be attributed to the reduction of power consumption and the generation of large number of bubbles to facilitate demulsification.

The comparison of performance and energy consumption of different demulsification and separation approaches is shown in **Table S3**. The electroflotation coupled membrane separation (ECM) technology proposed in this study exhibits excellent demulsification and separation performance of above 99.9%, which significantly exceeds electroflocculation, aeration, chemical demulsification, media coalescence, ultrasonic, and freeze-thaw approaches (40%-98%). In addition, the optimized energy consumption of this work is 5.33 kWh m^{-3}, which is only 2.5-58% of

these approaches. Meanwhile, compared to the traditional electric field demulsification, the energy consumption of the ECM technology is greatly reduced due to the lower voltage applied, which is about one order of magnitude lower than that of the traditional approaches (**Table S3**). Therefore, the ECM technology is highly competitive in oil-water emulsion separation for its high efficiency and low energy consumption.

In comparison with other representative electro-enhanced membrane separation approaches in oil-water separation (**Table S4**), the ECM technology exhibits relatively high separation efficiency and flux. It is worth noting that many electrophoretic-dominated electro-enhanced membrane separation approaches generate only trace amounts of bubbles, which severely limit their utility in the demulsification process, and some also require additional pumping power to compensate for the low flux. In contrast, the ECM technology achieves significant improvement in demulsification efficiency and separation flux, even if accompanied with slightly increased energy consumption. This work is carried out in a high conductivity solution, and large amount of oxygen bubbles is generated, constituting an electroflotation-dominated efficient demulsification and separation. In the follow-up study, abundant oxygen bubbles will be utilized at the cathode side to generate active free radicals for effective degradation of surfactants and organic pollutants, realizing in situ complex wastewater treatment.

Energy consumption calculation

The energy consumption (E, kWh m^{-3}) for removal of oil with ECM process is calculated by **Eq. (S1)**.

$$E = \frac{UIt}{V \cdot 10^3} \quad \textbf{(S1)}$$

Where U is the voltage (V), I is the current (A), t is the time (h), and V is the volume of treated O/W emulsion (m^3). For low voltage continuous separation process, V is the filtrate volume, while for high voltage intermittent separation process, V additionally includes the volume of electroflotation treated emulsion in the upper layer.

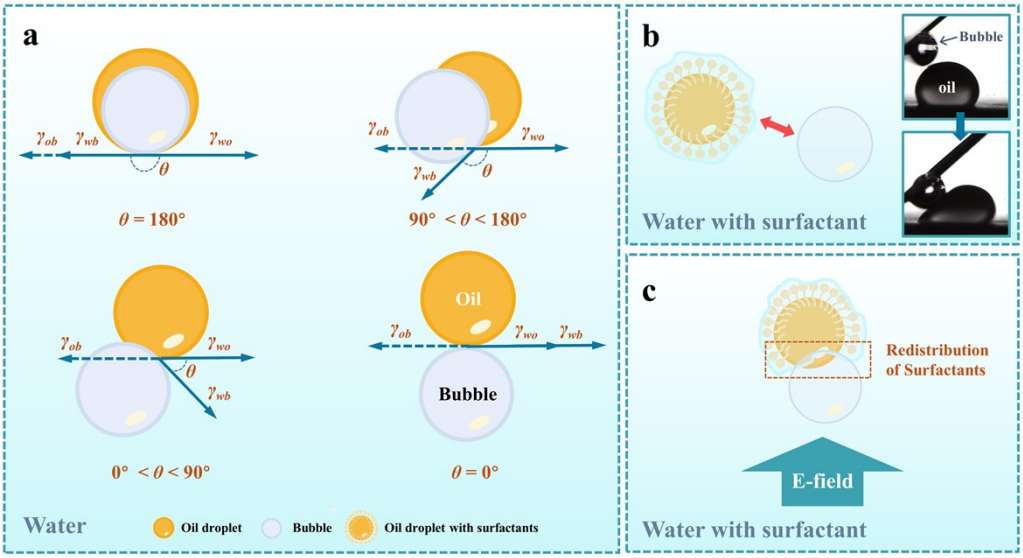

Scheme S1. (a) Schematic diagram of oil droplet-bubble attachment contact angle. (b) Schematic diagram of the resistance between microbubbles and emulsified oil droplets (insets show the photos of bubble and emulsified oil droplet that cannot spontaneously coalesce under water). (c) Schematic diagram of the interaction between microbubbles and emulsified oil droplets under electric field.

The difficulty of bubble-oil droplet attachment depends mainly on the surface property of the oil droplet.[S1] Oil droplets that are easily wetted by water on the surface are called hydrophilic, while those that are not easily wetted by water are hydrophobic. The wetting degree of oil droplets is usually described by the magnitude of the contact angle between bubbles and oil droplets in water (the angle between the gas-water interfacial tension line and the oil-water interfacial tension line). **Scheme S1a** shows the θ between the oil droplet and the bubble in water, and the tension of the three interfaces at the three-phase contact point is always in equilibrium:[S2]

$$\gamma_{wo} = \gamma_{ob} + \gamma_{wb}\cos(180° - \theta) \quad \textbf{(S2)}$$

where γ_{wo}, γ_{ob}, and γ_{wb} are the water-oil droplet, oil droplet-bubble, and water-bubble interfacial tensions, respectively. The interfacial energy (W) is the potential energy stored on the surface of colloid.[S3] The interfacial energy change (ΔW) when the bubble is in contact with the oil droplet is expressed as follow:

$$\Delta W = -\gamma_{wb}(1 + \cos(180° - \theta)) \quad \textbf{(S3)}$$

When in contact with bubbles, hydrophobic oil droplets with θ > 90° and $\Delta W < 0$ are prone to spontaneous adhesion, which is beneficial for air flotation. In contrast, hydrophilic oil droplets with θ < 90° and $\Delta W > 0$ do not easily adhere to bubbles.

The formula of bubbles collecting dispersed oil droplets probability (*P*)

The collision probability P_c can be calculated from the flow function under static condition and the microturbulence model under well-mixed condition:[S4, S5]

$$P_c = A(\frac{d_0}{d_b})^n \quad \textbf{(S4)}$$

$$A = 2/3 + (4Re^{0.75})/15, n = 2 \quad \textbf{(S5)}$$

where d_0 is the droplet diameter, d_b is the bubble diameter. The derived stream function of Yoon and Luttrell further confirmed the values of A and n (**Eq. (S5)**),[S6, S7] with A being positively correlated with Re.

The attachment probability is expressed in P_a.[S8]

$$P_a = sin^2\left\{2\arctan exp\left[\frac{-(45 + 8Re_b^{0.72})v_b t_i}{15d_b(\frac{d_b}{d_0} + 1)}\right]\right\} \quad \textbf{(S6)}$$

where v_b is the bubble rising velocity, t_i is the induction time, and t_c is the contact time (including collision time and sliding time). Attachment only occurs when t_i is less than t_c. Similarly, the liquid film behavior of the oil droplet spreading on bubbles can be determined based on the spreading coefficient S (**Eq. (S7)**).[S9] The spreading rate is proportional to S and decreases with increasing viscosity. Therefore, oils with higher viscosity, such as edible oils, do not spread easily on microbubbles and are difficult to separate by electroflotation.[S10]

$$S = \gamma_{wb} - (\gamma_{ob} + \gamma_{wo}) \quad \textbf{(S7)}$$

In a highly disordered condition, the oil droplet will separate from the bubble surface with the separation probability denoted by P_d.[S11]

$$P_d = exp(1 - \frac{6\gamma sin^2(\frac{\theta}{2}) d_b^{\frac{1}{3}}}{3.75 d_0^2 \rho_0 \varepsilon^{\frac{2}{3}}}) \quad \textbf{(S8)}$$

where θ is the contact angle, γ is the surface tension of the liquid, ε is the dissipation rate of mechanical energy, and ρ is the oil density.

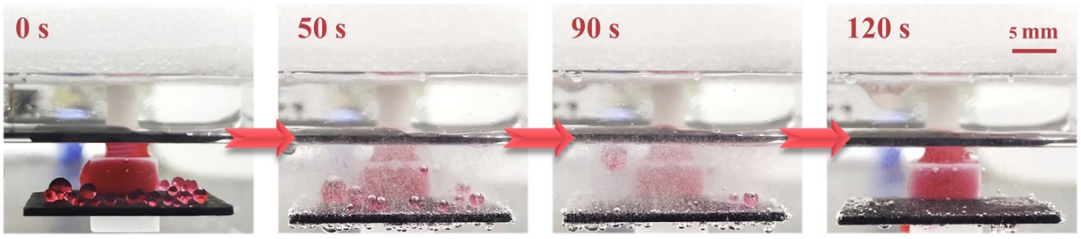

Fig. S9. Digital photos of the removal of stacked oil on CoTF surface via microbubbles at 10 V.

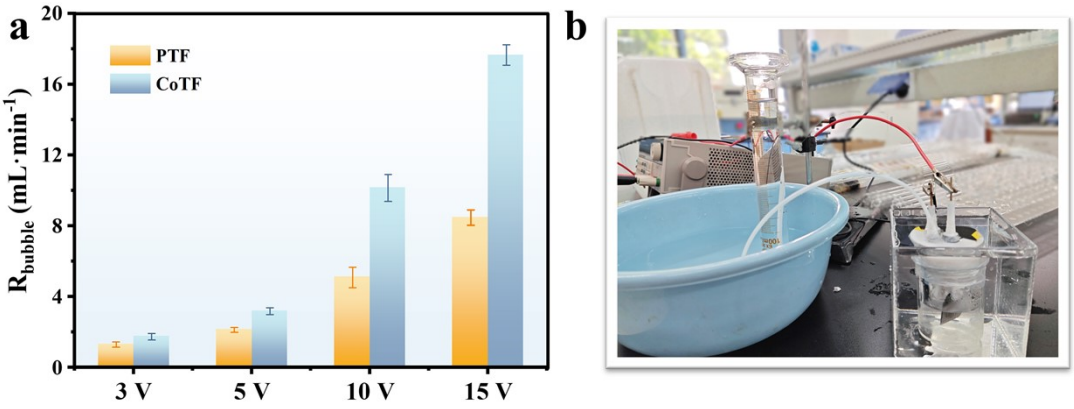

Fig. S10. (a) Bubble generation rates of PTF and CoTF at different voltages. (b) Photo of bubble collection device.

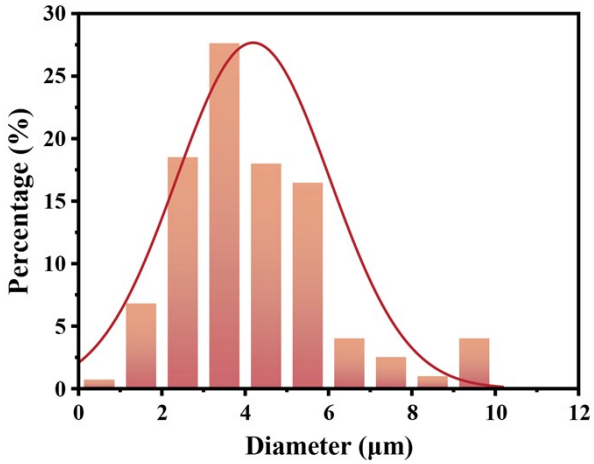

Fig. S11. Particle size distribution of as-prepared surfactant stabilized kerosene/water emulsion.

Table S1. Summary of the properties of the oils used in O/W emulsion separation (room temperature).

Oils	Viscosity (mPa s)	Density (g cm^{-3})	Surface tension (mN m^{-1})
Petroleum ether[a]	0.35	0.75	18.8
Isooctane[b]	0.53	0.6919	20.5
Kerosene[c]	2	0.80	32
Edible oil[S12]	53.68	0.90	35
1,2-dichloroethane[d]	0.84	1.2	25

[a]Data from the CRC Handbook of Chemistry and Physics.

[b]Data from the Merck Index-Encyclopedia of Chemicals, Drugs and Biologicals.

[c]Data from Material Safety Data Sheet SDS/MSDS CAS: 8008-20-6.

[d]Data from Material Safety Data Sheet SDS/MSDS CAS: 107-06-2.

Table S2. Comparison of the separation performance of various types of O/W emulsion separation materials

Membranes	Oil type	Running time	Flux ($L/(m^2 \cdot h \cdot bar)$)	Separation efficiency (%)	Ref.
PVDF/TAT/FS	toluene	20	4212.3	99.5	S13
PEG/MXene@MOF	crude oil	60	1246	99.7	S14
Sugarcane-based membranes	kerosene	-	1702	99.9	S15
MXene/TiONT (PMT)	n-hexane	-	578.7	99.7	S16
Attapulgite-based nanofiber	soybean oil	60	1121	99.2	S17
seaweed-like g-C_3N_4(SCN-2)	chloroform	-	3114	97.4	S18
PTFE/PLA	chloroform	-	5197	99.9	S19
Cu (−3V)	vacuum oil	30	2516	98	S20
GO@g-C_3N_4/NMB	cyclohexane	-	1611	99.21	S21
PVA/GO@MOF	crude oil	60	1020	99.3	S22
PA/PFHA/PPS	Pump oil	240	4100	98	S23
Cu^{2+}/alginate modified PAA-g-PVDF	hexadecane	60	1230	99.8	S24
MCOOH-CaTS/CO_3	n-hexane	200	3979.5	99.6	S25
water glass-bonded silicon carbide ceramic membrane	lubricant oil	60	234.8	98.9	S26
CoTF (0 V)	kerosene	-	2989.73	99.68	**This work**
CoTF (10 V)	kerosene	400	7604.32	99.9	

Table S3. Comparison of energy consumption and demulsification effect of different oily wastewater treatment technologies.

Approaches	Energy consumption (kWh m^{-3})	Demulsification efficiency (%)	Advantage	Disadvantage
Electric Field Coalescence[S27-S29]	54.1-124	76-99	Environmentally friendly, no secondary pollution	High energy consumption, potential safety hazards
Combination of Electric Field and Medium Coalescence[S30]	6.1-18.2	91.3-99.5	High separation efficiency, without scaling and clogging	Long residence time, sensitive parameters
Aeration and Electric Field Synergistic Demulsification[S31]	0.76 kWh	96.7	High separation efficiency	Complex equipment and high operation costs
Parallel plate Electrocoagulation[S32-S33]	9.1-41.9	93.97-97.07	High separation efficiency	Electrode passivation and high operation costs
Chemical Demulsification[S34]	52.5	98	Wide application range, high separation efficiency	High cost, environmental pollution, oil loss
Freeze-thaw method[S35]	42.9	80	No secondary pollution	Low energy efficiency
Ultrasonic Emulsion Separation[S36]	25	40	No secondary pollution	Low separation efficiency
Electroflotation Coupled Membrane Separation **(this work)**	5.33	99.9	High separation efficiency, low energy consumption	Immature equipment

Table S4. Comparison of representative electro-enhanced membrane separation approaches for oil-water separation.

Membranes	**Solution concentration**	**Bubble amount**	**Flux ($L\ m^{-2}\ h^{-1}\ bar^{-1}$)**	**Separation efficiency (%)**	**Energy consumption ($kWh\ m^{-3}$)**	**Ref.**
Cu membrane	1 g L^{-1} Na_2SO_4	few	2516	98	0.16	S37
TiO_2/TF	0.2 mM Na_2SO_4	few	7559	98.4	0.73	S38
Ni@PA	/	few	3000	91.4	3	S39
CoP/SSM	0.1 M Na_2SO_4	abundant	22480	98.6	3.18	S40
$TiSe_2$/TF	real seawater	abundant	2500	99	6.9	S41
NiTi-LDH/TF	real seawater	abundant	2600	99	8.7	S42
CoTF	0.2 M Na_2SO_4	abundant	7540	99.9	5.33	**This work**

References

S1. C. Wang, Y. Lü, C. Song, D. Zhang, F. Rong and L. He, *Sci. Total Environ.*, 2022, **845**, 157304.

S2. Y. Xing, X. Gui, L. Pan, B.-E. Pinchasik, Y. Cao, J. Liu, M. Kappl and H.-J. Butt, *Adv. Colloid Interface Sci.*, 2017, **246**, 105-132.

S3. C. Wang, Y. Lü, T. Ye and L. He, *J. Water Process Eng.*, 2023, **56**, 104351.

S4. J. Ralston, D. Fornasiero and R. Hayes, *Int. J. Miner. Process.*, 1999, **56**, 133-164.

S5. X. Li, X. Yan, J. Li, L. Wang, H. Zhang and Y. Cao, *Chem. Eng. Process*, 2021, **168**, 108554.

S6. R. H. Yoon and G. H. Luttrell, *Coal Preparation*, 1986, **2**, 179-192.

S7. R. H. Yoon and G. H. Luttrell, *Min. Proc. Ext. Met. Rev.*, 1989, **5**, 101-122.

S8. M. W. Lim, E. V. Lau and P. E. Poh, *J. Taiwan Inst. Chem. Eng.*, 2016, **68**, 192-200.

S9. H. Eilers and J. Korff, *Transactions of the Faraday Society*, 1940, **35**, 229-241.

S10. C. Grattoni, R. Moosai and R. A. Dawe, *Colloid Surface A*, 2003, **214**, 151-155.

S11. S. Gautam and G. J. Jameson, *Miner. Eng.*, 2019, **132**, 316-325.

S12. F. Reyes-García and G. A. Iglesias-Silva, *J. Chem. Eng. Data*, 2017, **62**, 2726-2739.

S13. L. Wang, J. Liu, R. Zhang, J. Wu, X. Tian, L. Chen, X. Dai, Y. Yan, J. Pan and J. Dai, *J. Membr. Sci.*, 2024, **691**, 122253.

S14. B. Xiang, J. Gong, Y. Sun, W. Yan, R. Jin and J. Li, *J. Membr. Sci.*, 2024, **691**, 122247.

S15. Y. Liu, T. Bai, S. Zhao, Z. Zhang, M. Feng, J. Zhang, D. Li and L. Feng, *J. Hazard. Mater.*, 2024, **461**, 132551.

S16. Q. Zeng, D. L. Zhao, L. Shen, H. Lin, N. Kong, L. Han, C. Chen, J. Teng, C. Tang and T.-S. Chung, *Chem. Eng. J.*, 2023, **474**, 145579.

S17. H. Mao, P. Xu, S. Zhou, Z. Fan, A. Xue, M. Li, Y. Zhao, A. Wang, Z. Wu and Y. Fan, *J. Membr. Sci.*, 2023, **683**, 121811.

S18. L. Li, C. Luo, X. Chen, N. Chu, L. Li, M. Chao and L. Yan, *Adv. Funct. Mater.*, 2023, **33**, 2213974.

S19. J. Chai, G. Wang, A. Zhang, X. Li, Z. Xu, J. Zhao and G. Zhao, *Chem. Eng. J.*, 2023, **461**, 141971.

S20. Y. Shi, Q. Zheng, L. Ding, F. Yang, W. Jin, C. Y. Tang and Y. Dong, *Environ. Sci. Technol.*, 2022, **56**, 4518-4530.

S21. Y. Wan, L. Ma, T. Wang, G. Zhang, X. Li, J. Liao, M. Jiang and L. Zhang, *J. Membr. Sci.*, 2023, **685**, 121922.

S22. B. Xiang, J. Gong, Y. Sun and J. Li, *J. Hazard. Mater.*, 2024, **462**, 132803.

S23. C. Yang, Z. Wang, M. Long, B. Qin, Y. Wang, K. Zhi, Y. Zheng, J. Zhao, W. Li, Z. Wang, M. Zhang, R. Zhang, H. Wu and Z. Jiang, *J. Membr. Sci.*, 2023, **679**, 121690.

S24. S. Gao, Y. Zhu, J. Wang, F. Zhang, J. Li and J. Jin, *Adv. Funct. Mater.*, 2018, **28**, 1801944.

S25. X. Long, Y. Zheng, J. Hu, W. Luo, K. Han and F. Jiao, *Chem. Eng. J.*, 2024, **482**, 148971.
S26. Q. Jiang, B. Lin, Z. Zhong, Y. Fan and W. Xing, *J. Membr. Sci.*, 2024, **692**, 122311.
S27. A. T. Yasir, A. H. Hawari, M. Talhami, M. Baune, J. Thöming and F. Du, *J. Electrostat*., 2023, **122**, 103796.
S28. B. Ren and Y. Kang, *Langmuir*, 2018, **34**, 8923-8931.
S29. B. Ren and Y. Kang, *Sep. Purif. Technol.*, 2019, **211**, 958-965.
S30. H. Lu, Z. Pan, Z. Miao, X. Xu, S. Wu, Y. Liu, H. Wang and Q. Yang, *Chem. Eng. J. Adv.*, 2021, **6**, 100103.
S31. M. Yao, X. Dong, Z. Ran, H. Pan, T. Chen and Z. Ju, *J. Environ. Chem. Eng.*, 2024, **12**, 113365.
S32. M. P. M. Combatt, W. C. S. Amorim, E. M. d. S. Brito, A. F. Cupertino, R. C. S. Mendonça and H. A. Pereira, *Comput. Electron. Agric.*, 2020, **177**, 105676.
S33. Y. Liu, W.-m. Jiang, J. Yang, Y.-x. Li, M.-c. Chen and J.-n. Li, *Chemosphere*, 2017, **181**, 142-149.
S34. V. K. Rajak, I. Singh, A. Kumar and A. Mandal, *Pet. Sci. Technol.*, 2016, **34**, 1026-1032.
S35. W. Feng, Y. Yin, M. de Lourdes Mendoza, L. Wang, X. Chen, Y. Liu, L. Cai and L. Zhang, *J. Cleaner Prod.*, 2017, **148**, 84-89.
S36. X. Luo, H. Gong, J. Cao, H. Yin, Y. Yan and L. He, *Chem. Eng. Sci.*, 2019, **203**, 285-292.
S37. Y. Shi, Q. Zheng, L. Ding, F. Yang, W. Jin, C. Y. Tang and Y. Dong, *Environ. Sci. Technol.*, 2022, **56**, 4518-4530.
S38. X. Li, H. Lan, G. Zhang, X. Tan and H. Liu, *Environ. Sci. Technol.*, 2022, **56**, 4151-4161.
S39. Y. Gu, Q. Xia, B. Liu, Y. Zhao, L. Pu, J. Ding, Y. Liu, E. Li, C. D. Vecitis and G. Gao, *Environ. Sci. Technol.*, 2024, **58**, 20277-20288.
S40. H. Li, J. Zhang, S. Gan, X. Liu, L. Zhu, F. Xia, X. Luo and Q. Xue, *Adv. Funct. Mater.*, 2023, **33**, 2212582.
S41. X. Lu, L. Shen, Q. Zeng, J. Du, C. Chen, J. Teng, W. Yu, Y. Xu and H. Lin, *J. Membr. Sci.*, 2024, **692**, 122310.
S42. X. Lu, C. Chen, H. Lin, Q. Zeng, J. Du, L. Han, J. Teng, W. Yu, Y. Xu and L. Shen, *Small*, 2024, **20**, 2400205.